SIMULATION OF LOCAL FAILURE OF CONCRETE PLATES ON THE BASIS OF ERROR CONTROL

R. Lackner and H.A. Mang
Institute for Strength of Materials, Vienna University of Technology, Austria

Abstract

This paper reports on the simulation of localized failure by means of the finite element method (FEM). The quality of results is controlled by estimating the error and adapting the mesh accordingly. An incremental error measure applicable to elastoplastic problems is employed. It forms the basis for adaptive mesh refinement (AMR). For the generation of the mesh, the advancing front technique is employed. This technique is extended to permit an alignment of the mesh, which may be important in case of localization. Attempting to preserve the objectivity of the FE results for this case, the fictitious crack concept is employed. Its influence on the adaptive calculation scheme, including the restart of the computation at a certain load level, is discussed. The transfer of variables on the basis of the proposed calculation strategy is illustrated by means of two example problems. The impact of different prescribed error thresholds on the ultimate load is discussed in the third example.

Key words: localization, error estimation, concrete, adaptive FEM, transfer of variables

1 Introduction

Local failure, such as cracking of concrete, is characterized by narrow regions at which further deformations tend to concentrate. For the numerical simulation of localization within the framework of the FEM, the question of the objectivity of the results is a topic of ongoing research. Several concepts were developed in the past to achieve objective FE simulations of localization in real-life structures. The fictitious crack concept has proved to be reasonably well suited for this kind of simulations. The influence of changing the size of the element on the FE results is considerably reduced. Nevertheless, the direction of the crack propagation and, consequently, the load-bearing capacity of the structure are not entirely independent of the discretization (see, e.g., (Huemer et al. 1998))[1].

Further improvement of the numerical results is accomplished by remeshing techniques in the context of AMR. It is controlled either by element enrichment criteria (see e.g. (Deb et al. 1996)), aiming at a high mesh density in the localization area, or by error estimation. The latter form requires the definition of an error estimator. In view of the ill-posedness of the underlying mathematical problem, heuristic considerations appear to be an acceptable basis for the choice of a suitable error extimator. The background of pertinent estimators are modified versions of the smoothening technique proposed by Zienkiewicz and Zhu (1987) for elastic problems, see, e.g., (Perić et al. 1994).

In this paper an error estimator developed for elastoplastic material behavior is extended to application to localization problems. For a detailed description of the employed smoothening technique and the design of the new mesh the reader is referred to (Lackner and Mang 1998). The remainder of the paper is organized as follows: Chapter 2 deals with the modelling of localization (in form of cracks) in the context of the FEM. The employed adaptive strategy, containing the definition of the error estimator, the calculation strategy and the transfer of state variables from the old to the new mesh, is described in Chapter 3. Chapter 4 contains numerical examples showing the impact of the transfer of state variables on the load-bearing behavior and the simulation of localized failure of a cylinder splitting test. Concluding remarks are made in Chapter 5.

---

[1]This dependence should not be confused with the classical mesh dependence of FE results which, however, must lead to the correct result in the practically unattainable "limit of finite discretizations".

2 Modelling of cracks within the framework of the FEM

2.1 Material model for plain concrete

For the description of the material response of concrete, a multi-surface plasticity model is employed. It requires the definition of a space of admissible stress states, given by $\mathbb{E}=\{\boldsymbol{\sigma}:f_k(\boldsymbol{\sigma},\alpha_k)\leq 0 \text{ for } k=1,..N\}$, where N is the number of yield surfaces $f_k(\boldsymbol{\sigma},\alpha_k)$, with $\boldsymbol{\sigma}$ representing the stress tensor and α_k standing for a strain-like internal variable associated with the k-th yield surface. For the simulation of cracks the maximum principal stress (Rankine) criterion is used:

$$f_{RK}(\boldsymbol{\sigma},q_{RK}) = \left[\sqrt{\boldsymbol{\sigma}^T\mathbf{P}_{RK}\boldsymbol{\sigma}} + \boldsymbol{\sigma}^T\mathbf{p}_{RK}\right] - \left[f_{tu} - q_{RK}(\alpha_{RK})\right], \quad (1)$$

where q_{RK} is a stress-like internal variable, $\mathbf{P}_{RK}$ is a projection matrix, $\mathbf{p}_{RK}$ is a projection vector, and f_{tu} denotes the uniaxial tensile strength. The ductile behavior of concrete subjected to compressive loading is described by the Drucker-Prager plasticity model,

$$f_{DP}(\boldsymbol{\sigma},q_{DP}) = \left[\sqrt{\boldsymbol{\sigma}^T\mathbf{P}_{DP}\boldsymbol{\sigma}} + \boldsymbol{\sigma}^T\mathbf{p}_{DP}\right] - \left[f_{cy} - q_{DP}(\alpha_{DP})\right], \quad (2)$$

with f_{cy} representing the uniaxial elastic limit. q_{DP}, $\mathbf{P}_{DP}$ and $\mathbf{p}_{DP}$ are analogous to q_{RK}, $\mathbf{P}_{RK}$ and $\mathbf{p}_{RK}$. For the definition of the employed projection matrices and vectors, see, e.g., (Feenstra 1993) for the Rankine and (Lackner 1995) for the Drucker-Prager criterion. The respective evolutions of the yield strength during plastic loading are illustrated in Figure 1. They are derived on the basis of experimental observations (see (Van Vliet and Van Mier 1996), (Jansen and Shah 1997)). Both relations are calibrated according to the fictitious crack concept, which will be described in the following chapter.

2.2 Finite element representation; fictitious crack concept

The FEM is based on the algebraic form of the weak formulation of the underlying boundary value problem. In the case of cracking, the displacement field exhibits jumps, $[\![\mathbf{u}]\!]$, in the analytical solution. To preserve the continuity of the displacement field in the FE formulation the discrete crack is simulated by plastic strains distributed over a finite width. Three different ways of distribution have been proposed in the literature:

- a continuous distribution of plastic strains controlled by a nonlocal theory of plasticity (De Borst and Mühlhaus 1992),
- an element-embedded representation of cracks by defining the zone of plastic evolution within the finite element (Sluys and Berends 1998), and
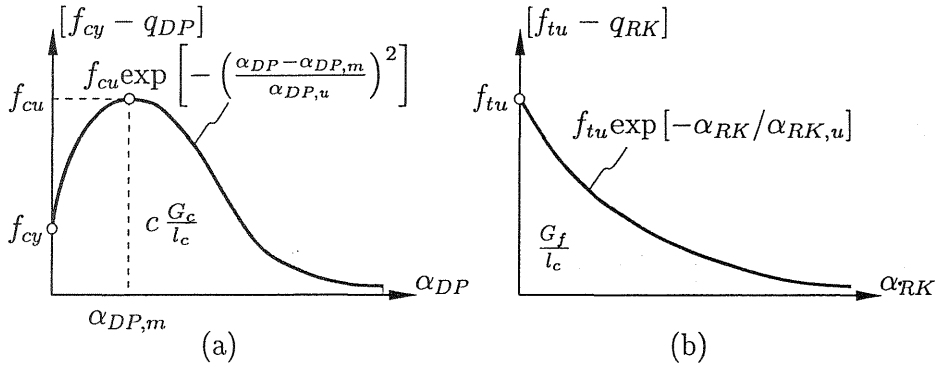
Fig. 1. Material model for concrete: hardening/softening relation for (a) compressive and (b) tensile loading. Both relations are calibrated according to the fictitious crack concept (G_c, G_f, c: material parameters, l_c: characteristic element size, $\alpha_{DP,u}, \alpha_{RK,u}$: calibration parameters)

- the fictitious crack concept using the entire element domain for the representation of the discrete crack (Oliver 1989).

Each of these approaches requires a length parameter for the definition of the plastic zone. It is computed according to the following condition:

The released fracture energy of the FE representation, $G_f^h = \int_t \{ \int_{V^{cr}} \boldsymbol{\sigma}^T \dot{\boldsymbol{\varepsilon}}^p dV \} d\tau$, must be equal to the released fracture energy obtained from a discrete crack, $G_f = \int_t \{ \int_{A^{cr}} \boldsymbol{\sigma}^T [\![\dot{\mathbf{u}}]\!] dA \} d\tau$.

Defining the characteristic length l_c as the ratio of the crack volume in the FE representation, V^{cr}, and the area of the discrete crack surface, A^{cr}, i.e., as

$$l_c = \frac{V^{cr}}{A^{cr}} \, , \tag{3}$$

the aforementioned condition yields

$$\int_{A^{cr}} \boldsymbol{\sigma}^T \left[\int_{l_c} \dot{\boldsymbol{\varepsilon}}^p dx_n - [\![\dot{\mathbf{u}}]\!] \right] dA = 0 \, , \tag{4}$$

where x_n denotes the local coordinate normal to the crack. In Equation (4), l_c represents the width of the plastic zone employed for the simulation of the crack. For the case of the fictitious crack concept, l_c is related to the element size. There are several ways of computing the characteristic length l_c as a function of the element size. They may be divided into two main groups:

- constant l_c,
- variable l_c, depending on the state of loading (e.g., on the direction of the relevant principal plastic strain).

Results from a comparative study of altogether five different approaches of determination of l_c were reported in (Huemer et al. 1998). The topic of this investigation was a bar under tensile loading. It was focussed on the artificial constraint of the deformation field caused by the FE representation of the crack. It was concluded that the approach proposed by Oliver (1989), which employs a singular band of finite elements for the definition of the crack, leads to the smallest constraint of this type. This approach is used herein.

The evaluation of the characteristic length l_c according to (Oliver 1989) is based on the crack orientation. Jumps of l_c occur in case of cracks rotating over node points of the element. Figure 2 illustrates this fact for a given element shape with varied crack orientation. Such
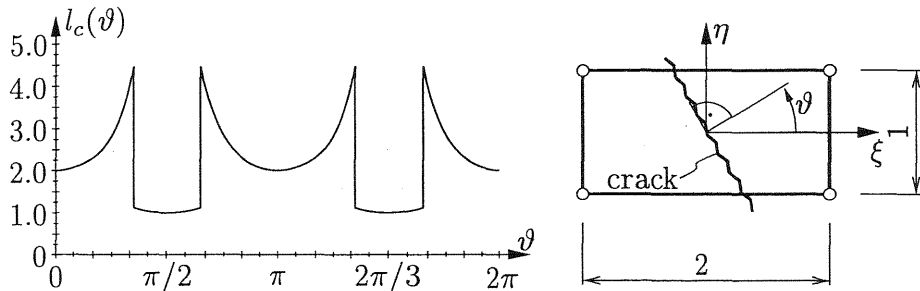

Fig. 2. Characteristic length l_c according to (Oliver 1989): dependence on the angle ϑ for a rotating crack within a given element geometry

discontinuities reduce the robustness of the implicit time-integration scheme. Hence, an explicit manner of defining the layout of the singular band is employed herein: l_c becomes a function of the plastic strains of the previous increment.

The rotation of the cracks causes changes of the characteristic length. The respective update of the characteristic length at the beginning of the load increment $n+1$, i.e., at $t=t_n$, results in changes in the softening relations. As shown in Figure 3, such a change yields a change in the material resistance $\bar{q}$. In order to avoid jumps in $\bar{q}$, a shift of the internal variable is performed. It is equal to $\alpha_{n+1}(t_n) - \alpha_n(t_n)$. As illustrated in Figure 3, the evolution of α contains jumps caused by the explicit update of l_c. Hence, $\alpha_n(t_n) \neq \sum_{i=1}^{n} \Delta\alpha_i(l_{c,i})$. The right-hand side of this inequality must be taken into account when computing quantities depending on the evolution of α.
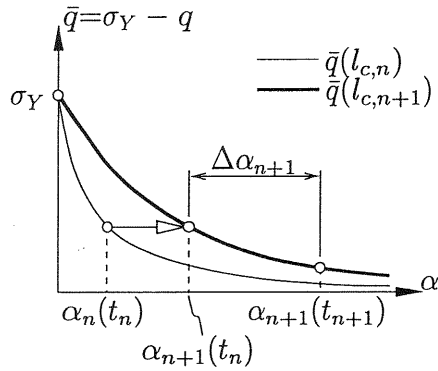
Fig. 3. Shift of the internal variable α in consequence of the variability of l_c

3 Adaptive FEM

This chapter contains a brief description of the proposed error estimator and the solution strategy. Special attention will be paid to the transfer of variables from the old to the new mesh, which is required as a consequence of the employed solution strategy.

3.1 Error estimator for elastoplasticity

The error estimator used herein is obtained by integration of the rate of an error measure over the respective time interval. The rates of the absolute error e and of the quantity u^h to which e is related are defined by:

$$(\dot{e^2}) = \int_V \sum_{i,j=1}^3 |\sigma_{ij}^* - \sigma_{ij}^h| \left[|\dot{\varepsilon}_{ij}^{e,*} - \dot{\varepsilon}_{ij}^{e,h}| + |\dot{\varepsilon}_{ij}^{p,*} - \dot{\varepsilon}_{ij}^{p,h}| \right] dV \qquad (5)$$

$$(\dot{u^{h,2}}) = \int_V \sum_{i,j=1}^3 |\sigma_{ij}^h| \left[|\dot{\varepsilon}_{ij}^{e,h}| + |\dot{\varepsilon}_{ij}^{p,h}| \right] dV \ . \qquad (6)$$

The quantities containing the superscript "h" are obtained from the FE calculation. The quantities containing the superscript "$*$" follow from post-processing based on a stress-smoothening technique proposed by Zienkiewicz and Zhu (1987), for details see (Lackner and Mang 1998). The employed relative incremental global error for the $(n+1)$-st increment, which is associated with the time interval $[t_n, t_{n+1}]$, is determined as follows:

$$\eta^2 = \frac{\int_{t_n}^{t_{n+1}} (\dot{e^2}) dt}{\int_{t_n}^{t_{n+1}} (\dot{u^{h,2}}) dt} \ . \qquad (7)$$

866

The mesh will only be refined after the error η exceeds a user-prescribed threshold value $\bar{\eta}$. The design of the new mesh is based on the advancing front technique aiming at an equal distribution of the local (element) error.

3.2 Solution strategy

According to the definition of the proposed incremental error estimator (Equation (7)) recomputations are restricted to the increments in which the error criterion has failed and, hence, the mesh was refined. After such a recomputation the analysis is continued through continuation of the load history. This approach requires the evaluation of initial quantities (displacements, stresses, internal variables, etc.) for the new mesh. Therefore, a transfer scheme is employed which will be described in detail in the following subchapter.

3.3 Transfer of variables

The transfer of variables provides the initial condition for the restart of the computation after mesh refinement. The left part of Table 1 contains the field variables associated with the old mesh. They were obtained from the FE analysis and from error estimation, respectively. The right part of Table 1 contains the required quantities associated with the new mesh. Whereas $\mathbf{u}$ and $\bar{\alpha}$ have to be transferred ($\bar{\alpha}$ are

Table 1. List of known quantities for the old mesh and required initial quantities for the new mesh

old mesh		new mesh
displacements $\mathbf{u}_{old}^{h}$ stresses $\boldsymbol{\sigma}_{old}^{h}$ (or $\boldsymbol{\sigma}_{old}^{*}$) plastic strains ε_{old}^{p} internal variables $\bar{\alpha}_{old}$	$\mapsto$	displacements $\mathbf{u}_{new}$ plastic strains ε_{new}^{p} internal variables $\bar{\alpha}_{new}$

scaled internal variables related to a constant reference length $\bar{l}_{c}$, see Section 3.3.3), only one of the two tensors $\boldsymbol{\sigma}$ and ε^{p} is required for the restart. The missing tensor is computed from the constitutive law,

(A) transfer of $\varepsilon^{p} \to \boldsymbol{\sigma}_{new}=\mathbf{C}(\varepsilon(\mathbf{u}_{new})-\varepsilon_{new}^{p})$, and
(B) transfer of $\boldsymbol{\sigma} \to \varepsilon_{new}^{p}=\varepsilon(\mathbf{u}_{new})-\mathbf{C}^{-1}\boldsymbol{\sigma}_{new}$ for $\bar{\alpha}_{new}{\neq}0$, else $\varepsilon^{p}{=}0$.

In general, the transferred pair of fields, $(\mathbf{u}_{new},\varepsilon_{new}^{p})$ or $(\mathbf{u}_{new},\boldsymbol{\sigma}_{new})$, does not yield an equilibrated state, i.e., $\mathbf{F}_{new}^{ext} - \mathbf{F}_{new}^{int}(\boldsymbol{\sigma}_{new}) \neq \mathbf{0}$, where $\mathbf{F}^{ext}$ and $\mathbf{F}^{int}$ denote the vector of external and internal forces, respectively. Hence, a global equilibrium iteration must be performed. The rate of convergence of this iteration is improved considerably if the

stress field is transferred (type (B) of transfer) because it is directly related to the vector of internal forces. The transfer of the two kinematic quantities $\mathbf{u}$ and ε^p, however, as it is the case with the transfer type (A), may lead to stress states which are far away from equilibrium. This results in a deterioration of the convergence behavior. In the following, the individual steps of transfer type (B), used in this work, will be discussed in detail.

3.3.1 Transfer of stresses (σ)

In this work the recovered stresses σ^*, computed during error estimation, are transferred to the new mesh. The stresses at the integration points of the new mesh are obtained by averaging the stresses from the old mesh over the proportionate areas of these points. The final values of the new stresses σ_{new} are obtained by an additional recovery of the transferred stresses within the new mesh.

3.3.2 Transfer of displacements ($\mathbf{u}$)

The displacement field for the new mesh is obtained by interpolation using the element shape functions. The transferred displacements do not match the stresses obtained from the transfer from the old to the new mesh. In order to eliminate this deficiency, a zero load step is performed, assuming the plastic flow to be frozen. The so-obtained displacements and stresses are referred to as $\tilde{\mathbf{u}}$ and $\tilde{\sigma}$, respectively.

3.3.3 Transfer of internal variables ($\bar{\alpha}$)

Two strategies were developed. The second is a consequence drawn from the deficiencies of the first one.

3.3.3.1 Original strategy

To preserve the value of $\bar{q}$ during this transfer, the internal variable α is scaled to an arbitrary reference length $\bar{l}_c$ (see Figure 4) before performing the transfer. For the transfer of α_k the same averaging technique as used for the transfer of stresses is employed. For an increase of the plastic zone this transfer yields a reduction of the value of the internal variable α_k, resulting in an artificial increase of the elastic material domain (see (Huemer et al. 1998)). This deficiency was the motivation for an improvement of the original strategy.

3.3.3.2 Improved strategy

This strategy is based on computing the internal variable from the respective yield condition, i.e., from $f_k(\tilde{\sigma}, \bar{\alpha}_k)=0$. In regions where unloading was encountered, characterized by $f_k<0$, $\bar{\alpha}_k$ is determined as described in Subsection 3.3.3.1.
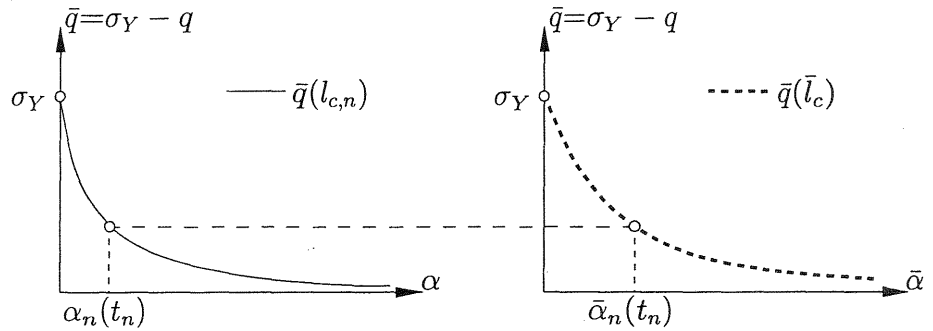
Fig. 4. Transfer of internal variables: introduction of a scaled internal variable $\bar{\alpha}$ related to a constant reference length $\bar{l}_c$

4 Numerical examples

The performance of the presented adaptive strategy is illustrated by means of three numerical examples. The emphasis of the first (bar under tension) and the second (L-shaped domain) example lies on the transfer of state variables from the old to the new mesh. For these examples the refinement is initiated after a constant time interval. The influence of restarting the computation at a certain point of time is investigated on the basis of the load-displacement diagram. Both strategies for the transfer of internal variables will be used. The third example (cylinder splitting test) illustrates the performance of adaptive analysis for different values of the user-prescribed error threshold, $\bar{\eta}$. Their influence on the ultimate load will be discussed.

4.1 Bar under tension

The academic example of a bar under tensile loading is chosen to illustrate the influence of the transfer scheme for the internal variable $\bar{\alpha}$ on the load-bearing behavior. The geometric dimensions and the material properties are given in Figure 5. The stress-strain diagram in the softening regime is assumed as bilinear. It is calibrated according to the fictitious crack concept. The simulation is carried out under displacement control. The mesh is adapted after equal intervals of the prescribed displacement ($\Delta \bar{u}{=}0.0005$ mm). No error estimation is performed for this example. The chosen meshes and their sequence of application are illustrated in Figure 6. The purpose of this sequence is to simulate the change of the size of the plastic zone. The onset of localization is triggered by the tensile strength f_{tu} in the elements containing the center of the bar (dark-shaded elements in Figure 6).

Figure 6 contains the load-displacement curves for the two transfer
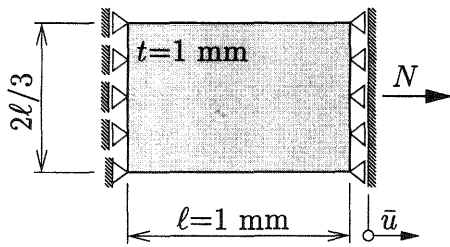
Fig. 5. Bar under tension: geometric dimensions and material properties

strategies. For the original transfer strategy the spreading of the plastic zone in the context of coarsening of the mesh leads to a stiffening of the structural response. The improved strategy gives the correct load-displacement relation.
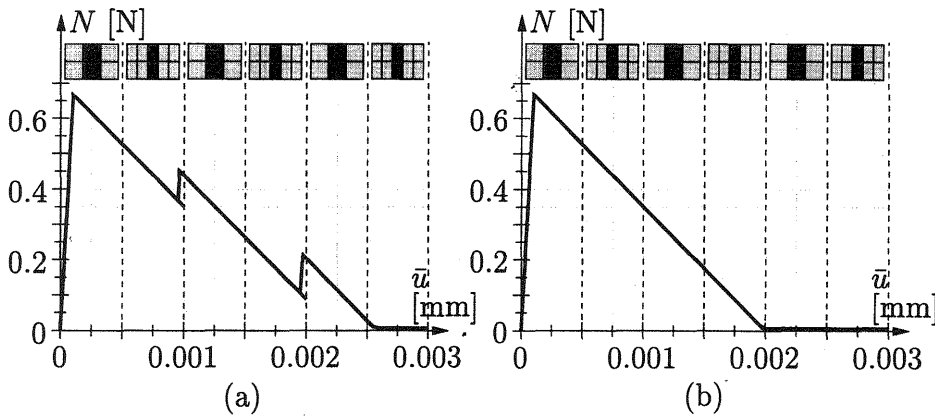

Fig. 6. Bar under tension: load-displacement diagram (with the respective FE meshes) for (a) the original strategy and (b) the improved strategy for the transfer of variables (change of mesh after $\Delta \bar{u}=0.0005$ mm)

4.2 L-shaped domain

In contrast to the first example, the crack initiation is determined by the shape of the plate. Hence, no triggering of the onset of localization is required. The dimensions of the plate and the material properties are given in Figure 7. The hardening/softening relation is chosen according to Subchapter 2.1. The mesh is refined at displacement intervals of $\Delta \bar{u}=0.2$ mm. Meshing is controlled by the local (element) error aimed at a constant number of elements, $m_e=250$. In addition to the adaptive calculation (referred to as multi-mesh calculation) the entire analysis is repeated with each one of the five meshes used in the adaptive analysis.

Figure 8 contains the obtained load-displacement curves. Again, artificial stiffening of the response in the softening regime is observed in case of the original strategy for the transfer of the internal variables (see Figure 8(a)). As regards the improved strategy for this transfer, this deficiency is almost eliminated (see Figure 8(b)). The relatively large differences between the curves obtained from single-mesh calculations indicate the limits of the fictitious crack concept and emphasize the relevance of adaptive analysis. These differences reflect the design

material properties:

$E = 10000$ N/mm^2

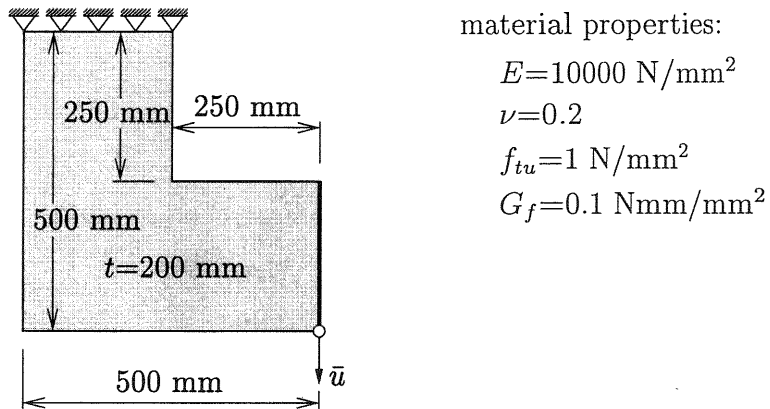$\nu = 0.2$

$f_{tu} = 1$ N/mm^2

$G_f = 0.1$ Nmm/mm^2

Fig. 7. L-shaped domain: geometric dimensions and material properties

of the meshes at different loading stages. These meshes are characterized by a refinement in the immediate vicinity of the crack tip and a coarsening of the mesh along the remaining part of the crack line.

4.3 Cylinder splitting test

The dimensions of the concrete cylinder and of the loading platens are shown in Figure 9 (ASCE/ACI Committee 447 1994). The material properties are given by: $E = 26200$ N/mm^2, $\nu = 0.2$, $f_{cu} = 30.3$ N/mm^2, $f_{tu} = 3.0$ N/mm^2, $G_f = 0.1$ Nmm/mm^2 and $G_c = 5.25$ Nmm/mm^2 for the concrete specimen, and $E = 11030$ N/mm^2 and $\nu = 0.2$ for the loading platens made of plywood.

Theoretical investigations concerning cylinder splitting tests were reported in (Bonzel 1964a). The tensile splitting strength of concrete, f_{tsu}, was determined from the formula

$$f_{tsu} = \frac{2\,P_u}{\pi\,d\,l}\;,\tag{8}$$

where P_u is the ultimate load and d and l are the diameter and the length of the concrete cylinder. Setting $f_{tsu} = f_{tu}/0.75$ according to
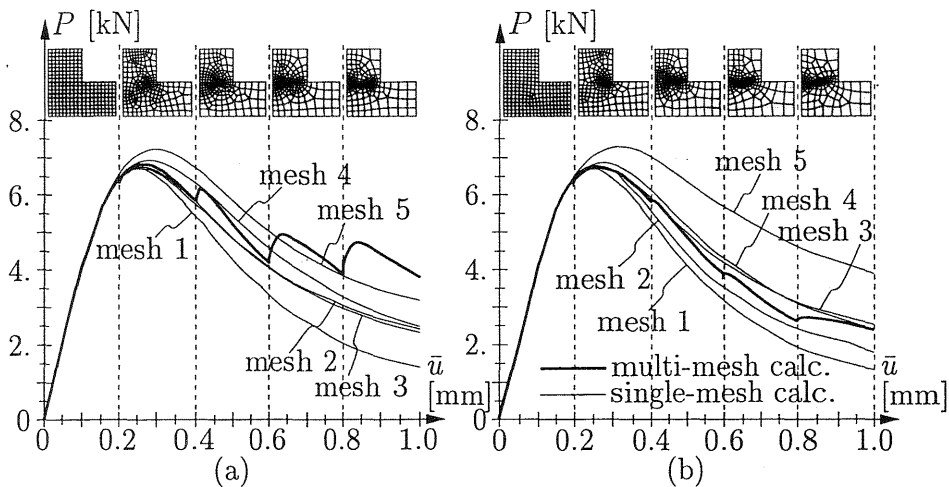
Fig. 8. L-shaped domain: load-displacement diagrams (with respective FE meshes) from adaptive (multi-mesh) and single-mesh calculations: (a) original strategy and and (b) improved strategy for the transfer of the internal variables

(Bonzel 1964b), the ultimate load for the considered specimen is estimated as

$$P_u = \frac{f_{tu}}{0.75} \frac{\pi \, d \, l}{2} = \frac{3.0}{0.75} \frac{\pi \cdot 152.4 \cdot 304.8}{2} = 292 \text{ kN} \; . \tag{9}$$

For the estimation of the error only the concrete specimen is considered.

The transfer of the internal variables is performed on the basis of the improved strategy.

Figure 10 shows error intervals in the form of grey-shaded columns. The upper bound of such an interval is the user-specified error tolerance, $\bar{\eta}$. The lower bound is the target error η^* needed for the design of the new mesh. Herein it is chosen as $0.9\bar{\eta}$. The ultimate load[2] P_u and the corresponding error η are plotted for different prescribed error thresholds, $\bar{\eta}$, listed in the second column of the table in Figure 10. For almost all simulations the obtained value of the error lies within the desired error interval $[\eta^*, \bar{\eta}]$. Convergence of the ultimate load P_u for decreasing values of $\bar{\eta}$ is observed.

---

[2]Because of symmetry of the system and the loading conditions, only one quarter of the cylinder was discretized. Hence, the obtained loads must be multiplied by 2 to obtain the ultimate load of the specimen.
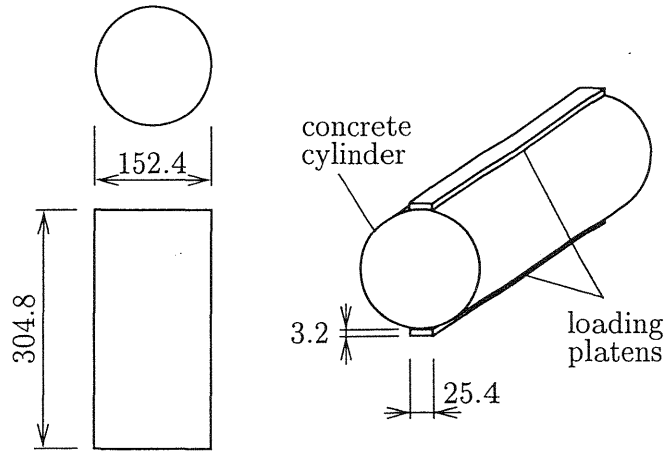
Fig. 9. Cylinder splitting test: dimensions (in [mm]) of the concrete specimen and of the loading platens made of plywood

The table in Figure 10 contains the values chosen for the error threshold and the target error, and the values obtained for the ultimate load and for the corresponding error together with the number of meshes, n_m, designed in the course of each simulation.

	$\bar{\eta}$ [%]	η^* [%]	P_u [kN]	η [%]	n_m [1]
●	20.00	18.00	153.3	18.51	2
■	17.50	15.75	154.1	15.62	2
▲	15.00	13.50	145.4	14.55	2
▼	12.50	11.25	141.8	10.80	3
○	10.00	9.00	137.5	8.12	4
□	7.50	6.75	138.5	7.41	4
△	5.00	4.50	131.9	4.98	5
▽	2.50	2.25	130.0	2.43	7

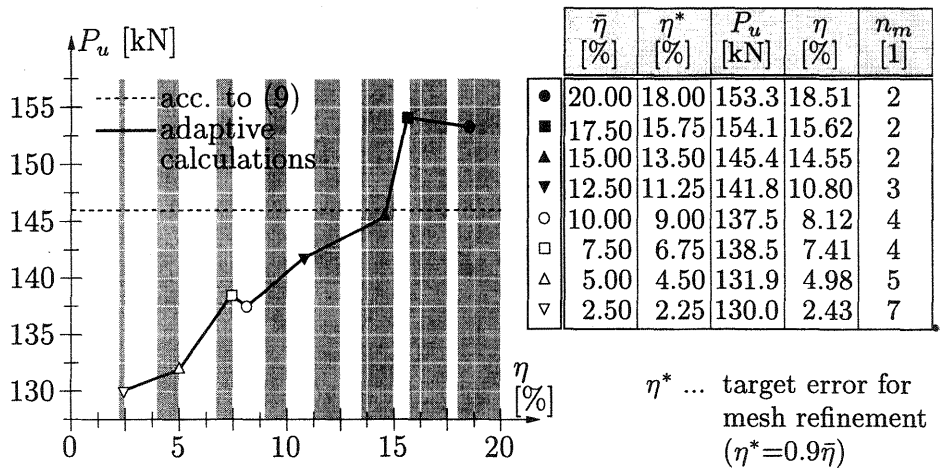η^* ... target error for mesh refinement $(\eta^*=0.9\bar{\eta})$

Fig. 10. Cylinder splitting test: ultimate load P_u and corresponding value of the error η for different values of $\bar{\eta}$. Number of meshes generated during the adaptive calculation: n_m.
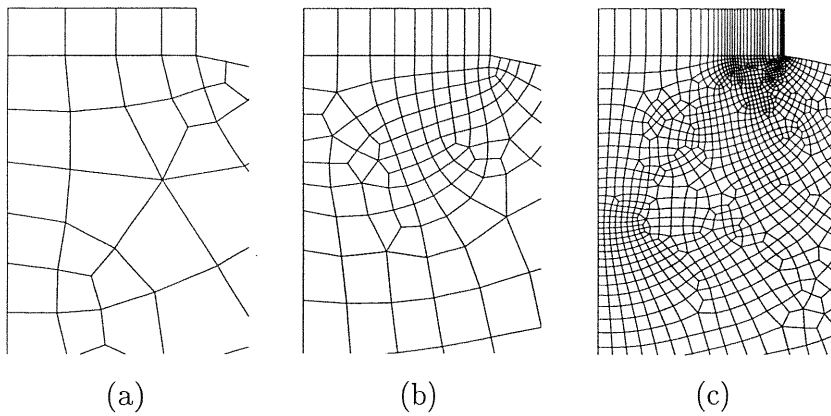
<div align="center">(a)   (b)   (c)</div>

Fig. 11. Cylinder splitting test: FE mesh used at the ultimate load for (a) $\bar{\eta}$=12.5% (67 elements), (b) $\bar{\eta}$=7.5% (270 elements) and (c) $\bar{\eta}$=2.5% (2193 elements)

Figure 11 shows the meshes used at the time instant corresponding to the ultimate load for three different values of the prescribed error tolerance. Obviously, the mesh density increases with decreasing values of $\bar{\eta}$. The discretization, designed on the basis of the employed error estimator, follows the failure mode at the vicinity of the loading platen.

5 Concluding remarks

This paper has dealt with the simulation of localized failure of plain concrete. For the purpose of controlling the error of the results, an adaptive calculation scheme was employed in the context of the FEM. The main items may be summarized as follows:

- As for the simulation of cracks within the framework of the FEM, the fictitious crack concept was employed. The characteristic length was taken as variable, computed according to (Oliver 1989).
- As for the error estimation, an incremental error measure applicable to elastoplastic material behavior was used.
- With regards to the solution strategy, the calculation was restarted at the load level at which the mesh was adapted. The transfer of the history variables was performed with the help of the constitutive relations, respectively, using the transferred stresses and displacements.
- The application of the proposed calculation strategy to the simulation of a cylinder splitting test indicated the convergence of the results for decreasing values of the user-prescribed error tolerance.

6 References

ASCE/ACI Committee 447 (1994). **Round-robin-test question-naire**. Technical report, Department of Civil, Environmental, and Architectural Engineering. University of Colorado, Boulder.

Bonzel, J. (1964a). Über die Spaltzugfestigkeit des Betons. **Beton**, 64(3), 108–114. In German.

Bonzel, J. (1964b). Über die Spaltzugfestigkeit des Betons (Fortsetzung). **Beton**, 64(4), 150–157. In German.

De Borst, R. and Mühlhaus, H. (1992). Gradient-dependent plasticity: Formulation and algorithmic aspects. **International Journal for Numerical Methods in Engineering**, 35, 521–539.

Deb, A., Prevost, J., and Loret, B. (1996). Adaptive meshing for dynamic strain localization. **Computer Methods in Applied Mechanics and Engineering**, 137, 285–306.

Feenstra, P. (1993). **Computational aspects of biaxial stress in reinforced concrete**. PhD thesis, Technical University Delft, The Netherlands.

Huemer, T., Lackner, R., and Mang, H. (1998). Implementation and application of an algorithm for adaptive finite element analysis of concrete plates. **Mechanics of Quasi-Brittle Materials and Structures** (eds. Bittnar, Z., Pijaudier-Cabot, G., and Gérard, B.), Prague, Czech Republic.

Jansen, D. and Shah, S. (1997). Effect of length on compressive strain softening of concrete. **Journal of Engineering Mechanics (ASCE)**, 123(1), 25–35.

Lackner, R. (1995). **Ein anisotropes Werkstoffmodell für Beton auf der Grundlage der Plastizitäts- und der Schädigungstheorie**. Master's thesis, University of Technology of Vienna, Austria. In German.

Lackner, R. and Mang, H. (1998). Adaptive FEM for the analysis of concrete structures. **Computational Modelling of Concrete Structures** (eds. de Borst, R., Bićanić, N., and Mang, H.), 2, 897–919, Badgastein, Austria. Balkema Publishers, Rotterdam.

Oliver, J. (1989). A consistent characteristic length for smeared cracking models. **International Journal for Numerical Methods in Engineering**, 28, 461–474.

Perić, D., Yu, J., and Owen, D. (1994). On error estimates and adaptivity in elastoplastic solids: Applications to the numerical simulation of strain localization in classical and Cosserat continua. **International Journal for Numerical Methods in Engineering**, 37, 1351–1379.

Sluys, L. and Berends, A. (1998). 2D/3D modelling of crack propagation with embedded discontinuity elements. **Computational Modelling of Concrete Structures** (eds. de Borst, R., Bićanić, N., and Mang, H.), 1, 399–408, Badgastein, Austria. Balkema Publishers, Rotterdam.

Van Vliet, M. and Van Mier, J. (1996). Experimental investigation of concrete fracture under uniaxial compression. **Mechanics of Cohesive-Frictional Materials**, 1, 115–127.

Zienkiewicz, O. and Zhu, J. (1987). A simple error estimator and adaptive procedure for practical engineering analysis. **International Journal for Numerical Methods in Engineering**, 24, 337–357.